

YOLOv6 v3.0: A Full-Scale Reloading

Chuyi Li* Lulu Li* Yifei Geng* Hongliang Jiang*
MengCheng Bo Zhang Zaidan Ke Xiaoming Xu† Xiangxiang Chu
Meituan Inc.

{lichuyi, lilulu05, gengyifei, jianghongliang02,
chengmeng05, zhangbo97, kezaidan, xuxiaoming04, chuxiangxiang}@meituan.com

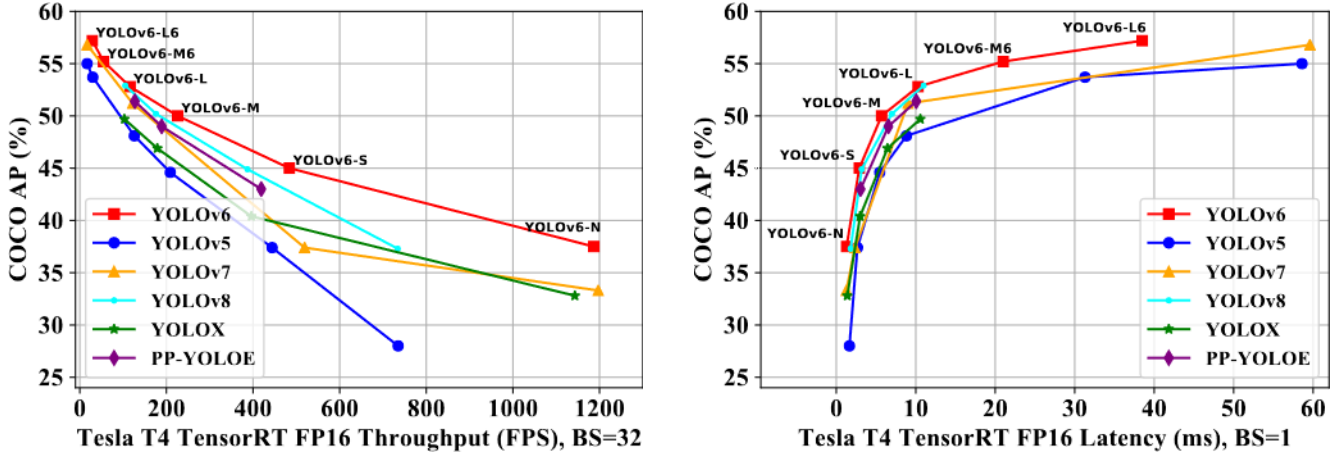


Figure 1: Comparison of state-of-the-art efficient object detectors. Both latency and throughput (at a batch size of 32) are given for a handy reference. All models are test with TensorRT 7.

Abstract

The YOLO community has been in high spirits since our first two releases! By the advent of Chinese New Year 2023, which sees the Year of the Rabbit, we refurbish YOLOv6 with numerous novel enhancements on the network architecture and the training scheme. This release is identified as YOLOv6 v3.0. For a glimpse of performance, our YOLOv6-N hits 37.5% AP on the COCO dataset at a throughput of 1187 FPS tested with an NVIDIA Tesla T4 GPU. YOLOv6-S strikes 45.0% AP at 484 FPS, outperforming other mainstream detectors at the same scale (YOLOv5-S, YOLOv8-S, YOLOX-S and PPYOLOE-S). Whereas, YOLOv6-M/L also achieve better accuracy performance (50.0%/52.8% respectively) than other detectors at a similar inference speed. Additionally, with an extended backbone and neck design, our YOLOv6-L6 achieves the state-of-the-art accuracy in real-time. Extensive experiments are carefully conducted to validate the effectiveness of each improving component. Our code is made available at [https://](https://github.com/meituan/YOLOv6)

* Equal contributions.

† Corresponding author.

github.com/meituan/YOLOv6.

1. Introduction

The YOLO series has been the most popular detection frameworks in industrial applications, for its excellent balance between speed and accuracy. Pioneering works of YOLO series are YOLOv1-3 [12–14], which blaze a new trail of one-stage detectors along with the later substantial improvements. YOLOv4 [1] reorganized the detection framework into several separate parts (backbone, neck and head), and verified bag-of-freebies and bag-of-specials at the time to design a framework suitable for training on a single GPU. At present, YOLOv5 [5], YOLOX [3], PPYOLOE [17], YOLOv7 [16] and most recently YOLOv8 [6] are all the competing candidates for efficient detectors to deploy.

In this release, we strenuously renovate the network design and the training strategy. We show the comparison of YOLOv6 with other peers at a similar scale in Fig. 1. The new features of YOLOv6 are summarized as follows:

- We renew the neck of the detector with a Bi-directional

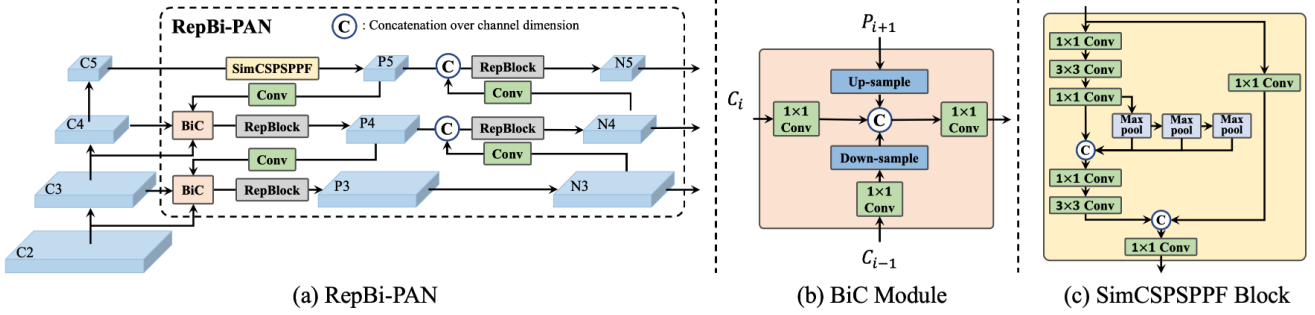


Figure 2: (a) The neck of YOLOv6 (N and S are shown). Note for M/L, RepBlocks is replaced with CSPStackRep. (b) The structure of a BiC module. (c) A SimCSPSPFF block.

Concatenation (BiC) module to provide more accurate localization signals. SPPF [5] is simplified to form the SimCSPSPFF Block, which brings performance gains with negligible speed degradation.

- We propose an *anchor-aided training* (AAT) strategy to enjoy the advantages of both anchor-based and anchor-free paradigms without touching inference efficiency.
- We deepen YOLOv6 to have another stage in the backbone and the neck, which reinforces it to hit a new state-of-the-art performance on the COCO dataset at a high-resolution input.
- We involve a new self-distillation strategy to boost the performance of small models of YOLOv6, in which the heavier branch for DFL [8] is taken as an *enhanced auxiliary regression branch* during training and is removed at inference to avoid the marked speed decline.

2. Method

2.1. Network Design

In practice, feature integration at multiple scales has been proven to be a critical and effective component of object detection. Feature Pyramid Network (FPN) [9] is proposed to aggregate the high-level semantic features and low-level features via a top-down pathway, which provides more accurate localization. Subsequently, there have been several works [2, 4, 10, 15] on Bi-directional FPN in order to enhance the ability of hierarchical feature representation. PANet [10] adds an extra bottom-up pathway on top of FPN to shorten the information path of low-level and top-level features, which facilitates the propagation of accurate signals from low-level features. BiFPN [15] introduces learnable weights for different input features and simplifies PAN to achieve better performance with high efficiency. PRB-FPN [2] is proposed to retain high-quality features for accurate localization by a parallel FP structure with bi-directional fusion and associated improvements.

Motivated by the above works, we design an enhanced-PAN as our detection neck. In order to augment localization signals without bringing in excessive computation burden, we propose a Bi-directional Concatenation (BiC) module to integrate feature maps of three adjacent layers, which fuses an extra low-level feature from backbone C_{i-1} into P_i (Fig. 2). In this case, more accurate localization signals can be preserved, which is significant for the localization of small objects.

Moreover, we simplify the SPPF block [5] to have a CSP-like version called SimCSPSPFF Block, which strengthens the representational ability. Particularly, we revise the SimSPPCSPC Block in [16] by shrinking the channels of hidden layers and retouching space pyramid pooling. In addition, we upgrade the CSPBlock with RepBlock (for small models) or CSPStackRep Block (for large models) and accordingly adjust the width and depth. The neck of YOLOv6 is denoted as RepBi-PAN, the framework of which is shown in Fig. 2.

2.2. Anchor-Aided Training

YOLOv6 is an anchor-free detector to pursue a higher inference speed. However, we experimentally find that the anchor-based paradigm brings additional performance gains on YOLOv6-N under the same settings when compared with the anchor-free one, as shown in Table 1. Moreover, anchor-based ATSS [18] is adopted as the warm-up label assignment strategy in the early versions of YOLOv6, which stabilizes the training.

Paradigm	AP^{val}	AP^s	AP^m	AP^l
Anchor-free	35.5%	16.0%	39.5%	51.0%
Anchor-based	35.6%	17.2%	39.8%	52.1%

Table 1: Comparisons of the anchor-free and the anchor-based paradigms on YOLOv6-N.

In light of this, we propose *anchor-aided training* (AAT), in which the *anchor-based auxiliary branches* are intro-

duced to combine the advantages of anchor-based and anchor-free paradigms. And they are applied both in the classification and the regression head. Fig. 3 shows the detection head with the auxiliaries.

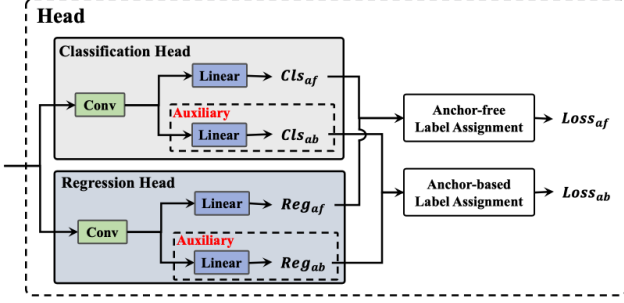


Figure 3: The detection head with anchor-based auxiliary branches during training. The auxiliary branches are removed at inference. ‘af’ and ‘ab’ are short for ‘anchor-free’ and ‘anchor-based’.

During the training stage, the auxiliary branches and the anchor-free branches learn from independent losses while signals are propagated altogether. Therefore, additional embedded guidance information from auxiliary branches is integrated into the main anchor-free heads. Worth mentioning that the auxiliary branches is removed at inference, which boosts the accuracy performance without decreasing speed.

2.3. Self-distillation

In early versions of YOLOv6, the self-distillation is only introduced in large models (i.e., YOLOv6-M/L), which applies the vanilla knowledge distillation technique by minimizing the KL-divergence between the class prediction of the teacher and the student. Meanwhile DFL [8] is adopted as regression loss to perform self-distillation on box regression similar to [19].

The knowledge distillation loss is formulated as:

$$L_{KD} = KL(p_t^{cls} || p_s^{cls}) + KL(p_t^{reg} || p_s^{reg}), \quad (1)$$

where p_t^{cls} and p_s^{cls} are class prediction of the teacher model and the student model respectively, and accordingly p_t^{reg} and p_s^{reg} are box regression predictions. The overall loss function is now formulated as:

$$L_{total} = L_{det} + \alpha L_{KD}, \quad (2)$$

where L_{det} is the detection loss computed with predictions and labels. The hyperparameter α is introduced to balance two losses. In the early stage of training, the soft labels from the teacher are easier to learn. As the training continues, the performance of the student will match the teacher so that the hard labels will help students more. Upon this, we apply *cosine weight decay* to α to dynamically adjust the

information from hard labels and soft ones from the teacher. The formulation of α is:

$$\alpha = -0.99 * ((1 - \cos(\pi * E_i / E_{max})) / 2) + 1, \quad (3)$$

where E_i denotes the current training epoch and E_{max} represents the maximum training epochs.

Notably, the introduction of DFL [8] requires extra parameters for the regression branch, which affects the inference speed of small models significantly. Therefore, we specifically design the *Decoupled Localization Distillation* (DLD) for our small models to boost performance without speed degradation. Specifically, we append a heavy auxiliary *enhanced regression branch* to incorporate DFL. During the self-distillation, the student is equipped with a naïve regression branch and the enhanced regression branch while the teacher only uses the auxiliary branch. Note that the naïve regression branch is only trained with hard labels while the auxiliary is updated according to signals from both the teacher and hard labels. After the distillation, the naïve regression branch is retained whilst the auxiliary branch is removed. With this strategy, the advantages of the heavy regression branch for DFL in distillation is considerably maintained without impacting the inference efficiency.

3. Experiments

3.1. Comparisons

The evaluation is made consistent with the early versions of YOLOv6 [7], which focuses on the throughput and the GPU latency at deployment. We test the speed performance of all official models with FP16-precision on the same Tesla T4 GPU with TensorRT [11]. We compare the upgraded YOLOv6 with YOLOv5 [5], YOLOX [3], PPYOLOE [17], YOLOv7 [16] and YOLOv8 [6]. Note that the performance of YOLOv7-Tiny is re-evaluated according to their open-sourced code and weights at the input size of 416 and 640. Results are shown in Table 2 and Fig. 1. Compared with YOLOv5-N/YOLOv7-Tiny (input size=416), our YOLOv6-N has significantly advanced by 9.5%/4.2% respectively. It also comes with the best speed performance in terms of both throughput and latency. Compared with YOLOX-S/PPYOLOE-S, YOLOv6-S can improve AP by 3.5%/0.9% with higher speed. YOLOv6-M outperforms YOLOv5-M by 4.6% higher AP with a similar speed, and it achieves 3.1%/1.0% higher AP than YOLOX-M/PPYOLOE-M at a higher speed. Besides, it is more accurate and faster than YOLOv5-L. YOLOv6-L is 3.1%/1.4% more accurate than YOLOX-L/PPYOLOE-L under the same latency constraint. Compared with the YOLOv8 series, our YOLOv6 achieves a similar performance in accuracy and in the latency for models at all sizes, while giving significant better throughput performance.

Method	Input Size	AP ^{val}	AP ^{val} ₅₀	FPS (bs=1)	FPS (bs=32)	Latency (bs=1)	Params	FLOPs
YOLOv5-N [5]	640	28.0%	45.7%	602	735	1.7 ms	1.9 M	4.5 G
YOLOv5-S [5]	640	37.4%	56.8%	376	444	2.7 ms	7.2 M	16.5 G
YOLOv5-M [5]	640	45.4%	64.1%	182	209	5.5 ms	21.2 M	49.0 G
YOLOv5-L [5]	640	49.0%	67.3%	113	126	8.8 ms	46.5 M	109.1 G
YOLOv5-N6 [5]	1280	36.0%	54.4%	172	175	5.8 ms	3.2 M	18.4 G
YOLOv5-S6 [5]	1280	44.8%	63.7%	103	103	9.7 ms	12.6 M	67.2 G
YOLOv5-M6 [5]	1280	51.3%	69.3%	49	48	20.1 ms	35.7 M	200.0 G
YOLOv5-L6 [5]	1280	53.7%	71.3%	32	30	31.3 ms	76.8 M	445.6 G
YOLOv5-X6 [5]	1280	55.0%	72.7%	17	17	58.6 ms	140.7 M	839.2 G
YOLOX-Tiny [3]	416	32.8%	50.3%*	717	1143	1.4 ms	5.1 M	6.5 G
YOLOX-S [3]	640	40.5%	59.3%*	333	396	3.0 ms	9.0 M	26.8 G
YOLOX-M [3]	640	46.9%	65.6%*	155	179	6.4 ms	25.3 M	73.8 G
YOLOX-L [3]	640	49.7%	68.0%*	94	103	10.6 ms	54.2 M	155.6 G
PPYOLOE-S [17]	640	43.1%	59.6%	327	419	3.1 ms	7.9 M	17.4 G
PPYOLOE-M [17]	640	49.0%	65.9%	152	189	6.6 ms	23.4 M	49.9 G
PPYOLOE-L [17]	640	51.4%	68.6%	101	127	10.1 ms	52.2 M	110.1 G
YOLOv7-Tiny [16]	416	33.3%*	49.9%*	787	1196	1.3 ms	6.2 M	5.8 G
YOLOv7-Tiny [16]	640	37.4%*	55.2%*	424	519	2.4 ms	6.2 M	13.7 G*
YOLOv7 [16]	640	51.2%	69.7%*	110	122	9.0 ms	36.9 M	104.7 G
YOLOv7-E6E [16]	1280	56.8%	74.4%*	16	17	59.6 ms	151.7 M	843.2 G
YOLOv8-N [6]	640	37.3%	52.6%*	561	734	1.8 ms	3.2 M	8.7 G
YOLOv8-S [6]	640	44.9%	61.8%*	311	387	3.2 ms	11.2 M	28.6 G
YOLOv8-M [6]	640	50.2%	67.2%*	143	176	7.0 ms	25.9 M	78.9 G
YOLOv8-L [6]	640	52.9%	69.8%*	91	105	11.0 ms	43.7 M	165.2 G
YOLOv6-N	640	37.0% / 37.5% [‡]	52.7% / 53.1% [‡]	779	1187	1.3 ms	4.7 M	11.4 G
YOLOv6-S	640	44.3% / 45.0% [‡]	61.2% / 61.8% [‡]	339	484	2.9 ms	18.5 M	45.3 G
YOLOv6-M	640	49.1% / 50.0% [‡]	66.1% / 66.9% [‡]	175	226	5.7 ms	34.9 M	85.8 G
YOLOv6-L	640	51.8% / 52.8% [‡]	69.2% / 70.3% [‡]	98	116	10.3 ms	59.6 M	150.7 G
YOLOv6-N6	1280	44.9%	61.5%	228	281	4.4 ms	10.4 M	49.8 G
YOLOv6-S6	1280	50.3%	67.7%	98	108	10.2 ms	41.4 M	198.0 G
YOLOv6-M6	1280	55.2% [‡]	72.4% [‡]	47	55	21.0 ms	79.6 M	379.5 G
YOLOv6-L6	1280	57.2% [‡]	74.5% [‡]	26	29	38.5 ms	140.4 M	673.4 G

Table 2: Comparisons with other YOLO-series detectors on COCO 2017 *val*. FPS and latency are measured in FP16-precision on a Tesla T4 in the same environment with TensorRT. All our models are trained for 300 epochs without pre-training or any external data. Both the accuracy and the speed performance of our models are evaluated with the input resolution of 640×640 . ‘[‡]’ represents that the proposed self-distillation method is utilized. ‘*’ represents the re-evaluated result of the released model through the official code.

To compare with the state-of-the-art methods, we follow [5] to add an extra stage on the top of the backbone to have a feature (C6) at a higher level for detecting extra-large objects. The neck is also expanded accordingly. The YOLOv6 of all sizes with C6 features are named YOLOv6-N6/S6/M6/L6 respectively. Further, the image resolution is adapted from 640 to 1280. The feature strides range from 8 to 64, which benefits the accurate detection for rather small and extra-large objects in high-resolution images. The experimental results listed in Table 2 show that the expanded YOLOv6 obtain significant gains in accuracy. Compared with expanded YOLOv5 (i.e., YOLOv5-N6/S6/M6/L6/X6), ours have a much higher AP at a similar inference speed.

When compared with the state-of-the-art YOLOv7-E6E, YOLOv6-L6 improves AP by 0.4% and runs 63% faster with a batch size of 1.

BiC+SimCSPSPPF	AAT	DLDD	AP ^{val}
✗	✗	✗	43.5%
✓	✗	✗	44.1%
✓	✓	✗	44.4%
✓	✓	✓	45.1%

Table 3: Ablation study for all designs on YOLOv6-S.

Model	BiC		AP^{val}	AP^s	AP^m	AP^l	FPS (bs=32)
	Bottom-up	Top-down					
YOLOv6-S	✗	✗	43.1%	23.4%	48.0%	59.9%	513
	✗	✓	43.7%	25.2%	48.7%	60.4%	492
	✓	✓	43.7%	25.0%	48.7%	59.7%	485
YOLOv6-L	✗	✗	50.9%	32.4%	56.0%	68.0%	125
	✗	✓	51.3%	34.2%	56.5%	67.6%	120
	✓	✓	51.1%	33.6%	56.7%	67.9%	119

Table 4: Effectiveness of the BiC module on YOLOv6.

3.2. Ablation Study

Experimental results in Table 3 exhibit the effectiveness of all contributions in this work. The renovated network with BiC and SimCSPSPFF has an enhanced AP by 0.6%. With AAT and DLD, the accuracy is further improved by 0.3% and 0.7% incrementally.

3.2.1 Network Design

We conduct a series of experiments to verify the effectiveness of the proposed BiC module. As can be seen in Table 4, applying the BiC module only on the top-down pathway of PAN brings 0.6%/0.4% AP improvements on YOLOv6-S/L respectively with negligible loss of efficiency. In contrast, when we try to import the BiC module into the bottom-up pathway, no positive gain in accuracy is obtained. The probable reason is that the BiC module on the bottom-up pathway would lead to confusion for detection heads about features at different scales. Therefore, we merely adopt the BiC module on the top-down pathway. Besides, the results indicate that the BiC module gives an impressive boost to the performance of small object detection. For both YOLOv6-S and YOLOv6-L, the detection performance on small objects is improved by 1.8%.

Further, we explore the influence of different types of SPP Blocks, including the simplified variants of SPPF [5] and SPPCSPC [16] (denoted as SimSPPF and SimSPPCSPC respectively) and our SimCSPSPFF blocks. Additionally, we apply SimSPPF blocks on the top three feature maps (P3, P4 and P5) of our backbone to verify its effectiveness, which is denoted as SimSPPF*3. Experimental results are shown in Table 5. We observe that heavily adopting SimSPPF brings little gain in accuracy with the increased computational complexity. SimSPPCSPC outperforms SimSPPF by 1.6%/0.3% AP on YOLOv6-N/S respectively while significantly decreasing inference speed. Compared with SimSPPF, our SimCSPSPFF version can obtain 1.1%/0.4%/0.1% performance gain for YOLOv6-N/S/M respectively. In terms of inference efficiency, our SimCSPSPFF block runs nearly 10% faster than SimSPPCSPC and is slightly slower than SimSPPF. For a better accuracy-efficiency trade-off, the SimCSPSPFF blocks are

introduced in YOLOv6-N/S. For YOLOv6-M/L, SimSPPF blocks are adopted.

Model	SPP Blocks	AP^{val}	FPS (bs=32)
YOLOv6-N	SimSPPF [5]	35.8%	1190
	SimSPPF [5]*3	35.9%	1072
	SimSPPCSPC [16]	37.4%	1078
	SimCSPSPFF	36.9%	1176
YOLOv6-S	SimSPPF [5]	43.7%	492
	SimSPPF [5]*3	43.6%	447
	SimSPPCSPC [16]	44.0%	432
	SimCSPSPFF	44.1%	477
YOLOv6-M	SimSPPF [5]	48.6%	227
	SimCSPSPFF	48.7%	218
YOLOv6-L	SimSPPF [5]	51.3%	120
	SimCSPSPFF	51.1%	117

Table 5: Ablation study on different types of SPP Blocks. All models are equipped with BiC modules.

3.2.2 Anchor-Aided Training

The advantages of the AAT is verified in YOLOv6. As shown in Table 6, it brings about 0.3%/0.5%/0.5% AP gain for YOLOv6-S/M/L respectively. Notably, the accuracy performance on small objects (AP^s) is significantly enhanced for YOLOv6-N/S/M. For YOLOv6-L, the performance on large objects (AP^l) is improved even further.

3.2.3 Self-distillation

We verify the proposed self-distillation method on YOLOv6-L. For a fair comparison, we also verified the model performance by doubling the training epochs besides the baseline since the self-distillation needs an extra entire training cycle to obtain the teacher model. As seen in Table 7, no performance improvement is attained without the weight decay strategy compared with the baseline. Doubling the training epochs is even worse due to overfitting.

Method	AAT	AP^{val}	AP^s	AP^m	AP^l
YOLOv6-N	✗	36.9%	17.2%	41.1%	52.9%
	✓	36.9%	18.7%	41.2%	53.0%
YOLOv6-S	✗	44.1%	24.7%	48.7%	61.1%
	✓	44.4%	25.4%	49.6%	60.2%
YOLOv6-M	✗	48.6%	29.7%	53.7%	65.5%
	✓	49.1%	31.1%	54.0%	65.4%
YOLOv6-L	✗	51.3%	34.2%	56.5%	67.6%
	✓	51.8%	33.4%	56.8%	68.8%

Table 6: Ablation study about AAT.

Model	Weight Decay	AP ^{val}
Baseline	-	51.8%
Double epochs	-	51.7%
Self-distillation	✗	51.8%
	✓	52.4%

Table 7: Ablation on the self-distillation on YOLOv6-L.

DLD	Double epochs	AP ^{val}
✗	✗	44.4%
✗	✓	44.6%
✓	✗	45.1%

Table 8: Ablation study of DLD on YOLOv6-S.

After the introduction of weight decay, the model is boosted by 0.6% AP.

In addition, the DLD specifically designed for small models is ablated on YOLOv6-S. As per self-distillation for large models, we also compare the results with the model trained with doubled epochs. As shown in Table 8, YOLOv6-S with DLD gives 0.7% AP boost and performs 0.5% better than that of training with doubled epochs.

4. Conclusion

In this report, YOLOv6 is upgraded on aspects of the network design and training strategy, which boost YOLOv6 to achieve the state-of-the-art accuracy for real-time object detection. In the future, we persistently work on the optimization of YOLOv6 to render an application-friendly detection framework as our research continues and the techniques in object detection advance.

References

- [1] Alexey Bochkovskiy, Chien-Yao Wang, and Hong-Yuan Mark Liao. Yolov4: Optimal speed and accuracy of object detection. *arXiv preprint arXiv:2004.10934*, 2020. **1**
- [2] Ping-Yang Chen, Ming-Ching Chang, Jun-Wei Hsieh, and Yong-Sheng Chen. Parallel residual bi-fusion feature pyramid network for accurate single-shot object detection. *IEEE Transactions on Image Processing*, 30:9099–9111, 2021. **2**
- [3] Zheng Ge, Songtao Liu, Feng Wang, Zeming Li, and Jian Sun. Yolox: Exceeding yolo series in 2021. *arXiv preprint arXiv:2107.08430*, 2021. **1, 3, 4, 7**
- [4] Golnaz Ghiasi, Tsung-Yi Lin, and Quoc V Le. Nas-fpn: Learning scalable feature pyramid architecture for object detection. In *Proceedings of the IEEE/CVF conference on computer vision and pattern recognition*, pages 7036–7045, 2019. **2**
- [5] Jocher Glenn. YOLOv5 release v6.1. <https://github.com/ultralytics/yolov5/releases/tag/v6.1>, 2022. **1, 2, 3, 4, 5, 7**
- [6] Jocher Glenn. Ultralytics YOLOv8. <https://github.com/ultralytics/ultralytics>, 2023. **1, 3, 4**
- [7] Chuyi Li, Lulu Li, Hongliang Jiang, Kaiheng Weng, Yifei Geng, Liang Li, Zaidan Ke, Qingyuan Li, Meng Cheng, Weiqiang Nie, et al. Yolov6: A single-stage object detection framework for industrial applications. *arXiv preprint arXiv:2209.02976*, 2022. **3**
- [8] Xiang Li, Wenhai Wang, Lijun Wu, Shuo Chen, Xiaolin Hu, Jun Li, Jinhui Tang, and Jian Yang. Generalized focal loss: Learning qualified and distributed bounding boxes for dense object detection. *Advances in Neural Information Processing Systems*, 33:21002–21012, 2020. **2, 3**
- [9] Tsung-Yi Lin, Piotr Dollár, Ross Girshick, Kaiming He, Bharath Hariharan, and Serge Belongie. Feature pyramid networks for object detection. In *Proceedings of the IEEE conference on computer vision and pattern recognition*, pages 2117–2125, 2017. **2**
- [10] Shu Liu, Lu Qi, Haifang Qin, Jianping Shi, and Jiaya Jia. Path aggregation network for instance segmentation. In *Proceedings of the IEEE conference on computer vision and pattern recognition*, pages 8759–8768, 2018. **2**
- [11] NVIDIA. TensorRT. <https://developer.nvidia.com/tensorrt>, 2018. **3**
- [12] Joseph Redmon, Santosh Divvala, Ross Girshick, and Ali Farhadi. You only look once: Unified, real-time object detection. In *Proceedings of the IEEE conference on computer vision and pattern recognition*, pages 779–788, 2016. **1**
- [13] Joseph Redmon and Ali Farhadi. Yolo9000: better, faster, stronger. In *Proceedings of the IEEE conference on computer vision and pattern recognition*, pages 7263–7271, 2017. **1**
- [14] Joseph Redmon and Ali Farhadi. Yolov3: An incremental improvement. *arXiv preprint arXiv:1804.02767*, 2018. **1**
- [15] Mingxing Tan, Ruoming Pang, and Quoc V Le. Efficientdet: Scalable and efficient object detection. In *Proceedings of the IEEE/CVF conference on computer vision and pattern recognition*, pages 10781–10790, 2020. **2**
- [16] Chien-Yao Wang, Alexey Bochkovskiy, and Hong-Yuan Mark Liao. Yolov7: Trainable bag-of-freebies sets new state-of-the-art for real-time object detectors. *arXiv preprint arXiv:2207.02696*, 2022. **1, 2, 3, 4, 5, 7**
- [17] Shangliang Xu, Xinxin Wang, Wenyu Lv, Qinyao Chang, Cheng Cui, Kaipeng Deng, Guanzhong Wang, Qingqing Dang, Shengyu Wei, Yuning Du, et al. Pp-yoloe: An evolved version of yolo. *arXiv preprint arXiv:2203.16250*, 2022. **1, 3, 4, 7**
- [18] Shifeng Zhang, Cheng Chi, Yongqiang Yao, Zhen Lei, and Stan Z. Li. Bridging the gap between anchor-based and anchor-free detection via adaptive training sample selection. In *CVPR*, 2020. **2**
- [19] Zhaohui Zheng, Rongguang Ye, Qibin Hou, Dongwei Ren, Ping Wang, Wangmeng Zuo, and Ming-Ming Cheng. Localization distillation for object detection. *arXiv preprint arXiv:2204.05957*, 2022. **3**

A. Detailed Latency and Throughput Benchmark

A.1. Setup

Unless otherwise stated, all the reported latency is measured on an NVIDIA Tesla T4 GPU with TensorRT version 7.2.1.6. Due to the large variance of the hardware and software settings, we re-measure latency and throughput of all the models under the same configuration (both hardware and software). For a handy reference, we also switch TensorRT versions (Table 9) for consistency check. Latency on a V100 GPU (Table 10) is included for a convenient comparison. This gives us a full spectrum view of state-of-the-art detectors.

A.2. T4 GPU Latency Table with TensorRT 8

See Table 9. The throughput of YOLOv6 models still emulates their peers.

Method	FPS (bs=1)	FPS (bs=32)	Latency (bs=1)
YOLOv5-N [5]	702	843	1.4 ms
YOLOv5-S [5]	433	515	2.3 ms
YOLOv5-M [5]	202	235	4.9 ms
YOLOv5-L [5]	126	137	7.9 ms
YOLOX-Tiny [3]	766	1393	1.3 ms
YOLOX-S [3]	313	489	2.6 ms
YOLOX-M [3]	159	204	5.3 ms
YOLOX-L [3]	104	117	9.0 ms
PPYOLOE-S [17]	357	493	2.8 ms
PPYOLOE-M [17]	163	210	6.1 ms
PPYOLOE-L [17]	110	145	9.1 ms
YOLOv7-Tiny [16]	464	568	2.1 ms
YOLOv7 [16]	128	135	7.6 ms
YOLOv6-N	785	1215	1.3 ms
YOLOv6-S	345	498	2.9 ms
YOLOv6-M	178	238	5.6 ms
YOLOv6-L	105	125	9.5 ms

Table 9: YOLO-series comparison of latency and throughput on a T4 GPU with a higher version of TensorRT (8.2).

A.3. V100 GPU Latency Table

See Table 10. The speed advantage of YOLOv6 is largely maintained.

A.4. CPU Latency

We evaluate the performance of our models and other competitors on a 2.6 GHz Intel Core i7 CPU using OpenCV Deep Neural Network (DNN), as shown in Table 11.

Method	FPS (bs=1)	FPS (bs=32)	Latency (bs=1)
YOLOv5-N [5]	577	1727	1.4 ms
YOLOv5-S [5]	449	1249	1.7 ms
YOLOv5-M [5]	271	698	3.0 ms
YOLOv5-L [5]	178	440	4.7 ms
YOLOX-Tiny [3]	569	2883	1.4 ms
YOLOX-S [3]	386	1206	2.0 ms
YOLOX-M [3]	245	600	3.4 ms
YOLOX-L [3]	149	361	5.6 ms
PPYOLOE-S [17]	322	1050	2.4 ms
PPYOLOE-M [17]	222	566	4.0 ms
PPYOLOE-L [17]	153	406	5.5 ms
YOLOv7-Tiny [16]	453	1565	1.7 ms
YOLOv7 [16]	182	412	4.6 ms
YOLOv6-N	646	2660	1.2 ms
YOLOv6-S	399	1330	2.0 ms
YOLOv6-M	203	676	4.4 ms
YOLOv6-L	125	385	6.8 ms

Table 10: YOLO-series comparison of latency and throughput on a V100 GPU. We measure all models at FP16-precision with the input size 640×640 in the exact same environment.

Method	Input	Latency (bs=1)
YOLOv5-N [5]	640	118.9 ms
YOLOv5-S [5]	640	202.2 ms
YOLOX-Tiny [3]	416	144.2 ms
YOLOX-S [3]	640	164.6 ms
YOLOX-M [3]	640	357.9 ms
YOLOv7-Tiny [16]	640	137.5 ms
YOLOv6-N	640	60.3 ms
YOLOv6-S	640	148.0 ms
YOLOv6-M	640	269.3 ms

Table 11: YOLO-series comparison of latency on a typical CPU. We measure all models at FP32-precision with the input size 640×640 in the exact same environment.